Arabidopsis ABCG14 forms a homodimeric transporter for multiple cytokinins and mediates long-distance transport of isopentenyladenine-type cytokinins

Jiangzhe Zhao[1], Xiaojuan Deng[1], Jiayun Qian[1], Ting Liu[1], Min Ju[1], Juan Li[1], Qin Yang[1], Xiaoxian Zhu[1], Weiqiang Li[2], Chang-Jun Liu[3], Zhigang Jin[1] and Kewei Zhang[1,*]

[1]Institute of Plant Stress Adaptation and Genetic Enhancement, Zhejiang Provincial Key Laboratory of Biotechnology on Specialty Economic Plants, College of Chemistry and Life Sciences, Zhejiang Normal University, Jinhua, Zhejiang 321004, P.R. China

[2]Key Laboratory of Mollisols Agroecology, Northeast Institute of Geography and Agroecology, Chinese Academy of Sciences, No. 4888 Shengbei Street, Changchun 130102, China

[3]Biology Department, Brookhaven National Laboratory, Upton, NY 11973, USA

*Correspondence: Kewei Zhang (kwzhang@zjnu.edu.cn)

https://doi.org/10.1016/j.xplc.2022.100468

ABSTRACT

Cytokinins (CKs), primarily *trans*-zeatin (*t*Z) and isopentenyladenine (iP) types, play critical roles in plant growth, development, and various stress responses. Long-distance transport of *t*Z-type CKs meidated by *Arabidopsis* ATP-binding cassette transporter subfamily G14 (AtABCG14) has been well studied; however, less is known about the biochemical properties of AtABCG14 and its transporter activity toward iP-type CKs. Here we reveal the biochemical properties of AtABCG14 and provide evidence that it is also required for long-distance transport of iP-type CKs. AtABCG14 formed homodimers in human (*Homo sapiens*) HEK293T, tobacco (*Nicotiana tabacum*), and *Arabidopsis* cells. Transporter activity assays of AtABCG14 in *Arabidopsis*, tobacco, and yeast (*Saccharomyces cerevisiae*) showed that AtABCG14 may directly transport multiple CKs, including iP- and *t*Z-type species. AtABCG14 expression was induced by iP in a *t*Z-type CK-deficient double mutant (*cypDM*) of CYP735A1 and CYP735A2. The *atabcg14 cypDM* triple mutant exhibited stronger CK-deficiency phenotypes than *cypDM*. Hormone profiling, reciprocal grafting, and $^2H_6$-iP isotope tracer experiments showed that root-to-shoot and shoot-to-root long-distance transport of iP-type CKs were suppressed in *atabcg14 cypDM* and *atabcg14*. These results suggest that AtABCG14 participates in three steps of the circular long-distance transport of iP-type CKs: xylem loading in the root for shootward transport, phloem unloading in the shoot for shoot distribution, and phloem unloading in the root for root distribution. We found that AtABCG14 displays transporter activity toward multiple CK species and revealed its versatile roles in circular long-distance transport of iP-type CKs. These findings provide new insights into the transport mechanisms of CKs and other plant hormones.

Key words: half-size ABC transporter, homodimer, isopentenyladenine-type cytokinins, long-distance transport, circular transport

INTRODUCTION

Plant hormones are endogenous signaling molecules that regulate plant physiology at very low concentrations (Santner et al., 2009; Novák et al., 2017; Šimura et al., 2018). Cytokinins (CKs) are essential plant hormones involved in cell division, meristem formation, immunity, leaf senescence, and various stress responses (Sakakibara, 2005; Kieber and Schaller, 2018;

Cortleven et al., 2019). CKs mainly consist of four types: *trans*-zeatin (*tZ*), isopentenyladenine (iP), *cis*-zeatin (cZ), and dihydrozeatin (DHZ). In *Arabidopsis thaliana* or *Oryza sativa* (rice), the key enzymes involved in CK biosynthesis and catabolism are adenosine phosphate-isopentenyltransferase for iP-ribotide phosphate (iPRP) biosynthesis (Sakamoto et al., 2006; Matsumoto-Kitano et al., 2008), the cytochrome P450 enzymes CYP735A1 and CYP735A2 for conversion of iPRPs to *tZ*-ribotide phosphates (Kiba et al., 2013), the phosphoribohydrolase LONELY GUY for activation of iPRPs and *tZ*-ribotide phosphates to free iP and *tZ* (Kurakawa et al., 2007; Kuroha et al., 2009), and CK dehydrogenase for irreversible degradation (Ashikari et al., 2005; Bartrina et al., 2011). CK signal transduction in *Arabidopsis* is a multistep two-component response system comprising CK receptor histidine kinases, cytosol-to-nucleus transport protein histidine phosphotransfer proteins, and downstream Arabidopsis response regulators or CK response factors (Hwang and Sheen, 2001; Hwang et al., 2012).

After synthesis in certain cells, CKs must be transported to target cells by long-distance or cellular transport to activate signal transduction. It has been demonstrated that *tZ*-type CKs are transported from the root to the shoot via the xylem to regulate shoot growth, whereas iP-type CKs are transported from the shoot to the root to regulate root development (Hirose et al., 2007; Ko et al., 2014; Sasaki et al., 2014; Zhang et al., 2014; Sakakibara, 2020). ATP-binding cassette (ABC) transporter subfamily G14 (AtABCG14) participates in root xylem loading and shoot phloem distribution of root-synthesized *tZ*-type CKs in shootward transport in *Arabidopsis* (Ko et al., 2014; Zhang et al., 2014; Zhao et al., 2021). An ortholog of AtABCG14 in rice, OsABCG18, also functions as a transporter for root-to-shoot transport of *tZ*-type CKs (Zhao et al., 2019), suggesting that ABC transporters play a conserved role in transport of root-synthesized CKs. When CKs reach the target cells, CK transporters at the plasma membrane (PM) or endoplasmic reticulum (ER) membrane are responsible for short-range cellular CK transport and signaling. AZA-GUANINE RESISTANT (AZG), ABC subfamily I (ABCI), and purine permeases (PUPs) are thought to function as CK importers or exporters or as bidirectional traffic facilitators. AtAZG2 is located in the ER and PM and inhibits lateral root emergence by mediating CK cellular transport in *Arabidopsis* (Tessi et al., 2020). AtABCI19, AtABCI20, and AtABCI21 are involved in the CK response in the ER under transcriptional regulation of ELONGATED HYPOCOTYL 5 at the seedling stage in *Arabidopsis* (Kim et al., 2020). The OsPUP1 and OsPUP7 transporters are located in the ER and regulate CK homeostasis in rice cells (Qi and Xiong, 2013; Xiao et al., 2020). AtPUP14 and OsPUP4, acting as PM-localized CK importers, regulate cellular CK homoeostasis in *Arabidopsis* and rice, respectively (Zurcher et al., 2016; Xiao et al., 2019). However, the molecular mechanism of long-distance transport of iP-type CKs remains unknown (Lacombe and Achard, 2016).

ABC proteins include full-size, half-size, and soluble transporters, which contain two nucleotide-binding domains (NBDs) and two transmembrane domains (TMDs), one NBD and one TMD, or only NBDs, respectively (Rees et al., 2009; Banasiak and Jasiński, 2021). The intracellular loop domains between TMDs and NBDs transfer signals to coordinate ATP binding and hydrolysis with continued substrate transport (Juan-Carlos et al., 2021). Half-size ABC transporters must form homodimers or heterodimers (Rees et al., 2009; McFarlane et al., 2010; Banasiak and Jasiński, 2021). As a half-size transporter, AtABCG14 has been found to physically interact with AtABCG11 in *Arabidopsis* protoplasts, but the growth phenotypes of the *atabcg11* mutant were very different from those of the *atabcg14* mutant (Le Hir et al., 2013; Ko et al., 2014; Yang et al., 2022). Although physiological evidence supports the theory that AtABCG14 is essential for CK transport, biochemical evidence is still lacking. Therefore, characterization of the partner and substrates of AtABCG14 is essential for understanding the transport mechanisms of CKs.

In this study, we found that AtABCG14 forms homodimers in human (*Homo sapiens*) HEK293T, tobacco (*Nicotiana tabacum*), and *Arabidopsis* cells. Transporter activity assays in homologous and heterologous expression systems showed that AtABCG14 mediated the efflux transport of various CKs, including *tZ* and iP-type CK species. To eliminate conversion of iP-type CKs to *tZ*-type CKs, the double mutant (*cypDM*) of CYP735A1 and CYP735A2, in which *tZ*-type CKs were reduced by 95% (Kiba et al., 2013), was used to study the long-distance transport mechanisms of iP-type CKs. Based on phytohormone profiling, isotope tracer experiments, grafting, and xylem sap assays, AtABCG14 was revealed to be crucial for root-to-shoot translocation and shoot distribution of iP-type CKs. AtABCG14 was also essential for shoot-to-root long-distance transport of iP-type CKs. These results suggest that AtABCG14 systemically mediates long-distance circulation transport of iP-type CKs in vascular tissues for signal communication between the root and shoot of *Arabidopsis*.

RESULTS

AtABCG14 forms homodimers in human HEK293T, tobacco, and *Arabidopsis* cells

To determine whether AtABCG14 forms homodimers, we transiently co-expressed FLAG- and Myc-tagged AtABCG14 in human HEK293T cells. Proper expression of FLAG-AtABCG14 and Myc-AtABCG14 fusion proteins in human HEK293T cells was confirmed by western blotting (Figure 1A). Co-immunoprecipitation (coIP) assays showed that Myc-AtABCG14 pulled down FLAG-AtABCG14, whereas FLAG-AtABCG14 pulled down Myc-AtABCG14, suggesting that AtABCG14 forms homodimers to transport CKs (Figure 1A). To confirm that AtABCG14 forms homodimers in plants, GFP-AtABCG14 and Myc-AtABCG14 fusion proteins were transiently co-expressed in tobacco. Immunoblot analysis detected Myc-AtABCG14 in the immunocomplex pulled down by anti-GFP beads but not in the negative controls (Figure 1B and Supplemental Figure 1), indicating that AtABCG14 forms homodimers in plants. To confirm that AtABCG14 forms a homodimer in stable transgenic plants, we constructed *35S::Myc-AtABCG14* and transformed it into the *atabcg14* mutant. *35S::Myc-AtABCG14* largely complemented the CK-deficiency phenotypes of *atabcg14* (Supplemental Figure 2). *35S::GFP-AtABCG14* has been transformed previously into *atabcg14*, and the mutant phenotype was completely rescued (Zhang et al., 2014). With F1 generation plants of *35S::GFP-AtABCG14* and *35S::Myc-AtABCG14* transgenic plants in the *atabcg14* background, we verified homodimerization of AtABCG14. Immunoblot analysis detected Myc-AtABCG14 in the immunocomplex pulled down by
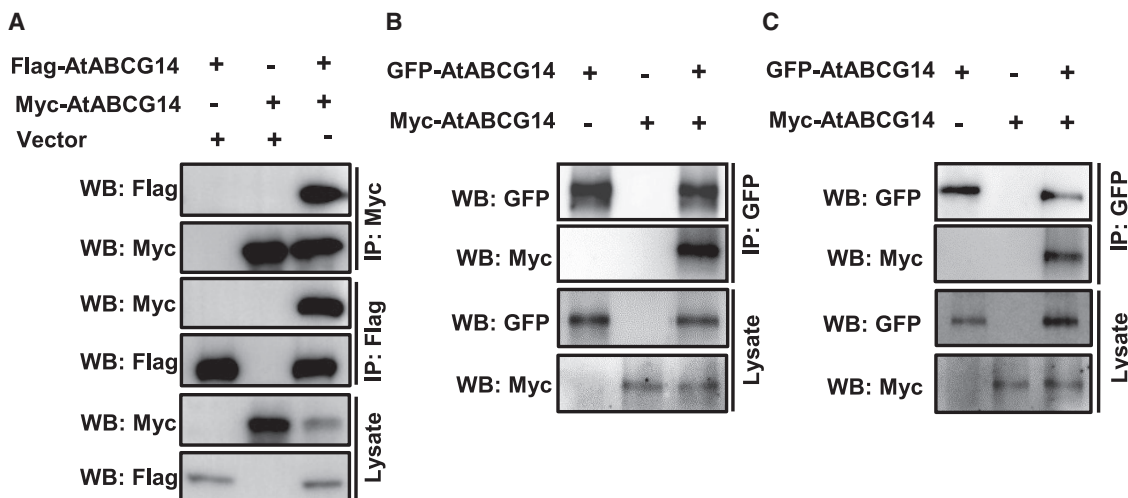
Figure 1. AtABCG14 forms homodimers *in vivo*.
(A) Reciprocal co-immunoprecipitation (coIP) assay of Myc-AtABCG14 and FLAG-AtABCG14 in human HEK293T cells. Total protein was extracted from human HEK293T cells transfected with *Myc-AtABCG14* and *FLAG-AtABCG14*.
(B and C) CoIP assay of GFP-AtABCG14 and Myc-AtABCG14 expression in tobacco leaves **(B)** and *Arabidopsis* **(C)**. Total protein was extracted from tobacco leaves **(B)** and 25-DAG transgenic plants **(C)** co-expressing *GFP-AtABCG14* and *Myc-AtABCG14*.

anti-GFP beads in protein extracts from F1 plants, but it was not detected in the *35S::GFP-AtABCG14* and *35S::Myc-AtABCG14* parent plants (Figure 1C). Our results revealed that AtABCG14 is capable of forming homodimers in human HEK293T cells and *in planta*.

AtABCG14 mediates efflux transport of multiple CK species

To measure the transporter activities of AtABCG14, we generated *35S::GFP-AtABCG14* transgenic tobacco BY-2 cell lines. qRT–PCR analysis and immunoblotting indicated that the GFP-AtABCG14 fusion protein was highly expressed in tobacco BY-2 cells (Supplemental Figure 3). Quantification of CKs in BY-2 cells showed that iPR, *tZ*-ribotide (*tZR*), *cZ*-ribotide (*cZR*), and *cZ* levels were significantly lower in BY-2 cells harboring GFP-AtABCG14 compared with the empty vector (Figure 2A). The levels of *tZR*, iPR, *cZ*, and *cZR* exported from BY-2 cells with GFP-AtABCG14 were higher than those exported from controls without GFP-AtABCG14 (Figure 2B). These results indicated that AtABCG14 displayed efflux transporter activities toward *tZR*, iPR, *cZR*, and *cZ*.

To confirm the transporter activity of AtABCG14 in *Arabidopsis* suspension cells, we generated calli from root segments of wild-type (WT) and *35S::GFP-AtABCG14* transgenic plants. Suspension cells induced from the calli were used for transporter activity assays. Quantification of CKs in the suspension cells showed that the levels of iP, iPR, *cZ*, and *cZR* were lower in *GFP-AtABCG14*-expressing suspension cells than in those of the controls (Figure 2C), whereas *tZ* and *tZR* levels were too low to be detected in the suspension cells. The exported CKs from the suspension cells were collected and quantified from 0.5–8 h (Figure 2D–2G). The levels of iP, iPR, *cZ*, and *cZR* secreted from the *GFP-AtABCG14*-expressing cells were significantly higher than those from the controls at different time points (0.5–8 h). Conversely, the levels of iP, iPR, and *cZR* were higher in the suspension cells of the *atabcg14* mutant but lower in the

culture medium compared with that of WT cells (Supplemental Figure 4). These results confirmed that AtABCG14 displayed efflux transporter activities toward iP, iPR, *cZ*, and *cZR*.

Transporter activity assays in a non-plant heterologous system can reveal the substrate of a plant-derived transporter. To gain insight into AtABCG14 transporter activities, we expressed the GFP-AtABCG14 fusion protein in *Saccharomyces cerevisiae* (yeast) strain YPH499 (Li et al., 2017). The fusion protein GFP-AtABCG14 with the correct size was detected by immunoblotting using a GFP antibody (Figure 3A). After incubation with various isotope-labeled CK substrates for 20 min, the yeast cells were collected by centrifugation and washed to remove substrates on the cell surface. The cellular CKs were extracted from the yeast cell pellet and measured by liquid chromatography-mass spectrometry (LC-MS). The levels of *tZ*, *tZR*, iPR, *cZ*, and DHZ in yeast cells expressing *GFP-AtABCG14* were significantly lower than those of the empty vector control (Figure 3B), indicating that AtABCG14 exhibited efflux transport activity toward these CKs. By contrast, efflux transport of these CKs from yeast cells was suppressed after treatment with sodium vanadate (an H^+-ATPase inhibitor) (Figure 3C). These results demonstrated that AtABCG14 may directly mediate the efflux of CKs.

To confirm the transport activity of AtABCG14 in yeast, we performed a time-dependent export experiment using $^2H_5$-*tZ* as a substrate. Yeast-expressed AtABCG14 exported high levels of $^2H_5$-*tZ* at 2, 4, 6, and 8 min (Figure 3D), confirming that AtABCG14 displays transport activity toward *tZ* in yeast. Therefore, using a heterologous expression system, we confirmed that AtABCG14 is directly involved in transport of multiple CK substrates, including iP-type species.

Expression of *AtABCG14* is induced by iP-type CKs

It has been demonstrated that the transcription of a transporter is generally induced by its substrates (Jasinski et al., 2001; Zhang et al., 2014). We therefore examined whether
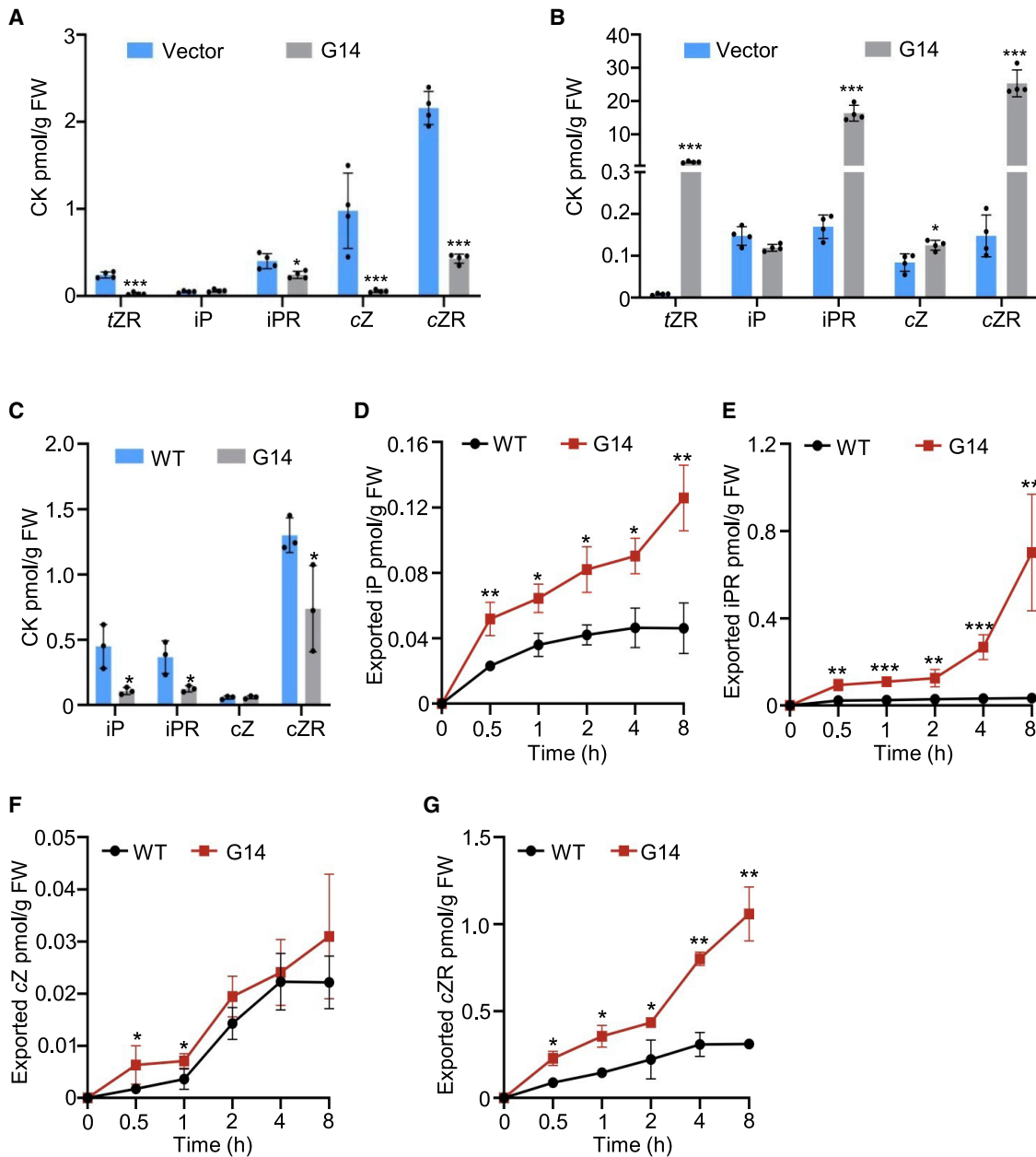
Figure 2. AtABCG14 displayed efflux transport activities toward multiple CK species in BY-2 cells and *Arabidopsis* cells.
(A) Quantification of *t*ZR, iP, iPR, *c*Z, and *c*ZR in BY-2 cells transformed with the *35S::GFP* (RCS2) and *35S::GFP-AtABCG14* vectors. BY-2 cells were collected 5 days after transfer to fresh culture medium. Data are means ± SD (*n* = 4).
(B) Quantification of *t*ZR, iP, iPR, *c*Z, and *c*ZR in BY-2 cells transformed with *35S::GFP* (RCS2) and *35S::GFP-AtABCG14*. Cells were collected 5 days after subculture. Data are means ± SD (*n* = 4).
(C) Quantification of iP, iPR, *c*Z, and *c*ZR in *Arabidopsis* cells transformed with *35S::GFP-AtABCG14* and WT cells 5 days after subculture. Data are means ± SD (*n* = 3).
(D–G) Quantification of the content of iP **(D)**, iPR **(E)**, *c*Z **(F)**, and *c*ZR **(G)** in *35S::GFP-AtABCG14* transformed *Arabidopsis* cells and WT cellscollected 5 days after subculture.
Data are means ± SD (*n* = 4). *$P < 0.05$, **$P < 0.001$, Student's *t*-test. *t*ZR, *trans*-zeatin ribotide; iP, isopentenyladenine; iPR, iP ribotide; *c*Z, *cis*-zeatin; *c*ZR, *c*Z ribotide; G14, AtABCG14; N.D., not detected; FW, fresh weight.

AtABCG14 was induced by iP-type CKs. *cypDM* is the double mutant of *cyp735a1* and *cyp735a2* and is defective in *trans*-hydroxylation, resulting in a significant reduction (95%) in *t*Z-type CKs and an increase in iP-type CKs *in planta* (Kiba et al., 2013). qRT–PCR analyses showed that the expression level of

AtABCG14 in *cypDM* was increased 1.8-fold compared with the WT (Supplemental Figure 5A). The expression level of *AtABCG14* in the *cypDM* mutant was significantly induced by iP treatment (Supplemental Figure 5B), suggesting that *AtABCG14* expression is directly induced by iP.
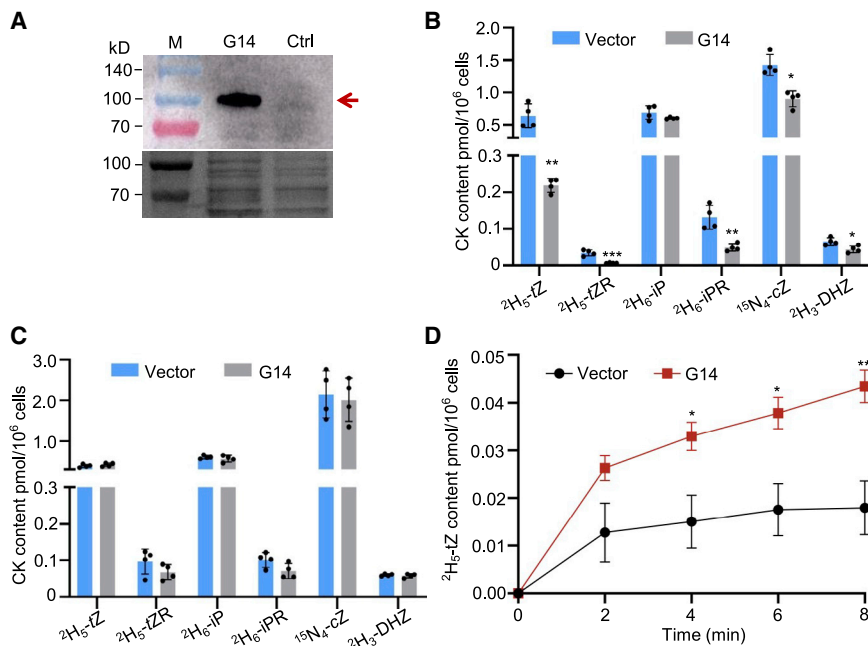
atabcg14 cypDM mutants show retardation of growth and development

To study the transport mechanism of AtABCG14 toward iP-type CKs, we generated the *atabcg14 cypDM* triple mutant by crossing *atabcg14* with the *cypDM* double mutant, thereby reducing the effect of *tZ* on the study of iP transport *in vivo* (Supplemental Figure 6). The roots of *atabcg14 cypDM* seedlings were substantially shorter than those of *cypDM* seedlings (Figure 4A and 4B). The chlorophyll content of cotyledon leaves was also significantly reduced in *atabcg14 cypDM* seedlings compared with *cypDM* seedlings (Figure 4A and 4C). The diameter of rosette leaves and the plant height were strikingly reduced in *atabcg14 cypDM* compared with *cypDM* (Figure 4D–4G). The number of primary branches was also significantly lower in *atabcg14 cypDM* compared with *cypDM* (Figure 4H). Finally, the number of siliques per plant was significantly reduced in *atabcg14 cypDM* triple mutants compared with *cypDM* (Figure 4I). Together, these results indicate that mutation of *AtABCG14* aggravated the CK-deficiency phenotype of *cypDM,* suggesting that AtABCG14 is responsible for transport of iP-type CKs *in planta*.

AtABCG14 is responsible for xylem loading of iP-type CKs in root-to-shoot translocation

To assess the role of AtABCG14 in translocation of iP-type CKs in *Arabidopsis*, we quantified CK levels in the shoot and root of *atabcg14 cypDM* mutant seedlings using *cypDM* as a control 8 days after germination (DAG). The levels of iPR were significantly reduced in the shoot (Figure 5A) but overaccumulated in the root of *atabcg14 cypDM* compared with *cypDM* (Figure 5B). These results demonstrated that AtABCG14 is involved in translocation of iP-type CKs from root to shoot.

To study the long-distance transport of iP-type CKs in *cypDM* and *atabcg14 cypDM*, we incubated the roots of *cypDM* and *atabcg14 cypDM* in medium containing 50 nM $^2H_6$-iP for 1 h. CK profiling

showed that the contents of $^2H_6$-iP and synthesized $^2H_6$-iPR were reduced by 81% and 72% in *atabcg14 cypDM* shoots compared with those of *cypDM* (Figure 5C), whereas the contents of $^2H_6$-iP and $^2H_6$-iPR in the roots of *cypDM* and *atabcg14 cypDM* did not differ significantly (Supplemental Figure 7). To exclude the effect of vasculature development on hormone transport, $^2H_6$-absisic acid (ABA) uptake was performed with seedlings of *cypDM* and *atabcg14 cypDM*. Shootward long-distance transport of $^2H_6$-ABA did not differ significantly between *cypDM* and *atabcg14 cypDM* (Supplemental Figure 8). These data confirm that AtABCG14 plays a crucial role in shootward long-distance transport of iP-type CKs.

To confirm that the shootward translocation of iP-type CKs is dependent on AtABCG14, we quantified the CK content in xylem sap from WT, *atabcg14*, *cypDM*, and *atabcg14 cypDM* plants at 25 DAG. The levels of iP-type CKs were significantly lower in xylem sap from *atabcg14 cypDM* than from *cypDM* plants (Figure 5D), implying that translocation of iP-type CKs from the root to the shoot was reduced in *atabcg14 cypDM* plants. The levels of iP and iPR in xylem sap from *atabcg14* plants were markedly lower than those in xylem sap from WT plants (Figure 5E). These findings suggest that AtABCG14 participates in xylem loading of iP-type CKs in root-to-shoot translocation.

AtABCG14 is responsible for phloem unloading of iP-type CKs in the shoot

To explore whether AtABCG14 participates in distribution of iP-type CKs in the shoot, *cypDM* and *atabcg14 cypDM* were grafted to generate chimeric plants with *atabcg14 cypDM* as the scion and *cypDM* as the rootstock (*atabcg14 cypDM/cypDM*) or vice versa (*cypDM/atabcg14 cypDM*). The diameters of the rosette leaves in the *atabcg14 cypDM/cypDM* and *cypDM/atabcg14 cypDM* heterografts were longer than those in the *atabcg14 cypDM/atabcg14 cypDM* homografts but shorter than those in the *cypDM/cypDM* homografts (Supplemental Figure 9A and
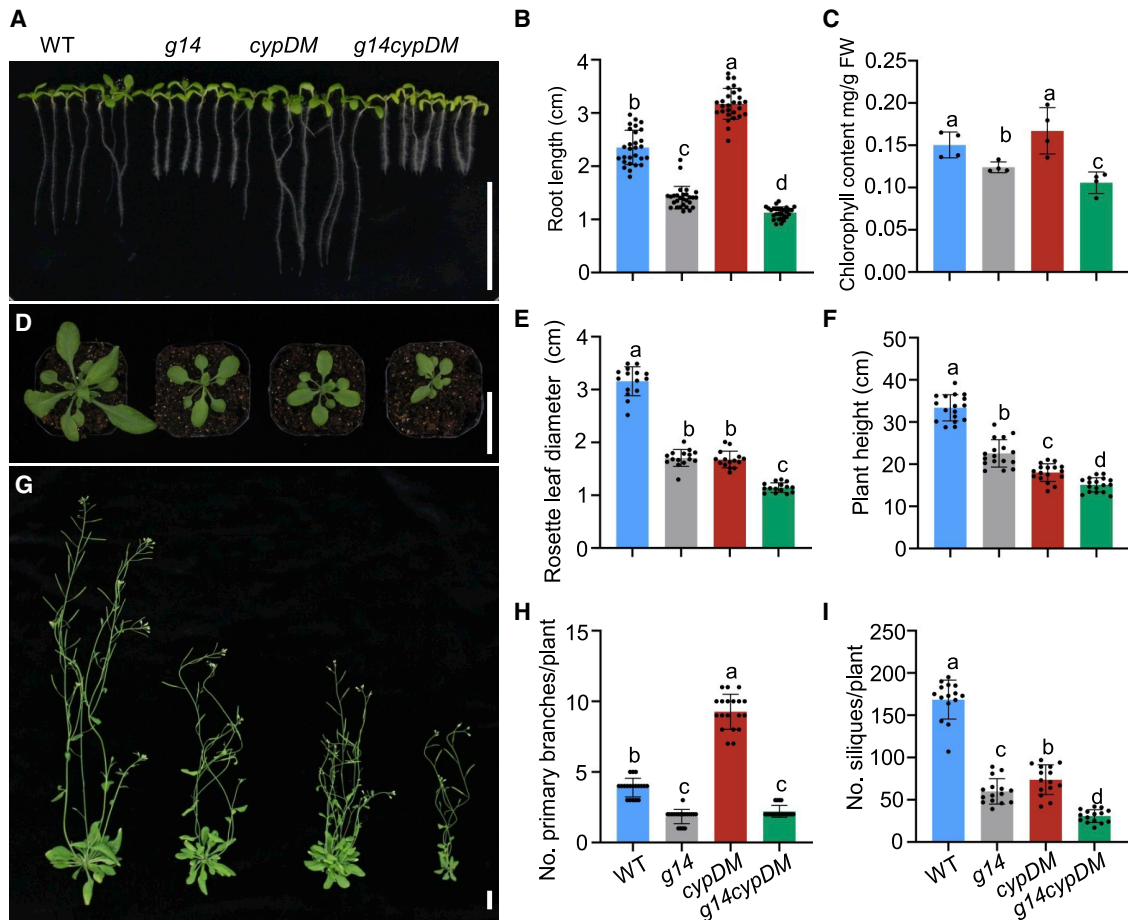
Figure 4. Morphological phenotype of the *atabcg14 cypDM* triple mutant line at different developmental stages.
(A) Phenotypes of the WT, *atabcg14*, *cypDM*, and *atabcg14 cypDM* 8 days after germination (DAG). Scale bar, 2 cm.
(B and C) Quantification of the root lengths **(B)** and chlorophyll contents **(C)** of the plants in **(A)**.
(D) Phenotypes of the WT, *atabcg14*, *cypDM*, and *atabcg14 cypDM* at 22 DAG. Scale bar, 2 cm.
(E) Quantification of rosette diameters of the plants in **(D)**.
(G) Phenotypes of the WT, *atabcg14*, *cypDM*, and *atabcg14 cypDM* at 35 DAG. Scale bar, 2 cm.
(F, H, and I) Quantification of plant height **(F)**, number of primary branches per plant **(H)**, and number of siliques per plant **(I)** of the plants in **(G)**.
Data are means ± SD. $n = 30$ in **(B)**, $n = 4$ in **(C)**, $n = 15$ in **(E)**, $n = 17$ in **(F)**, $n = 19$ in **(H)**, $n = 15$ in **(I)**. Groups marked with different letters are significantly different ($P < 0.05$, ANOVA). *g14cypDM* represents *atabcg14 cypDM*.

9C). Plant height, primary branch number, and silique number per plant were higher in these heterografts than in *atabcg14 cypDM/atabcg14 cypDM* but lower than in *cypDM/cypDM* (Supplemental Figure 9B and 9D–9F).

Consistent with the observed phenotypes, CK quantification showed that iP-type CK levels in the shoots of *atabcg14 cypDM/cypDM* and *cypDM/atabcg14 cypDM* heterografts were lower than those in *cypDM/cypDM* homografts but higher than those in *atabcg14 cypDM/atabcg14 cypDM* homografts (Figure 5F). Conversely, iP-type CK levels in the roots of *atabcg14 cypDM/cypDM* and *cypDM/atabcg14 cypDM* heterografts were higher than those in *cypDM/cypDM* homografts but lower than those in *atabcg14 cypDM/atabcg14 cypDM* homografts (Figure 5G). The phenotypes and iP-type CK levels of *atabcg14 cypDM/cypDM* grafted plants were only partially rescued to those of *cypDM/cypDM*, implying that *AtABCG14* expression in the shoot is required for shoot distribution of iP-type CKs.

To better understand the distribution of root-derived iP-type CKs in the shoot, apoplastic extracts and phloem sap of the grafted plants were collected and analyzed by LC-MS. The iP-type CKs were lower in the apoplastic extracts of *atabcg14 cypDM/atabcg14 cypDM* and *atabcg14 cypDM/cypDM* than in those of *cypDM/cypDM* and *cypDM/atabcg14 cypDM* (Figure 5H). The iP-type CK level was 4-fold higher in the phloem sap of *atabcg14 cypDM/cypDM* than in that of *cypDM/cypDM* grafts (Figure 5I), suggesting that AtABCG14 is involved in transport of iP-type CKs through the phloem and their distribution to the apoplast in the shoot. These data demonstrate that AtABCG14 is crucial for shoot distribution of iP-type CKs.

AtABCG14 is responsible for phloem unloading in the rootward transport of iP-type CKs

To understand whether AtABCG14 is involved in shoot-to-root transport of iP-type CKs, $^2H_6$-iP tracer experiments were performed. $^2H_6$-iP solution was dripped onto the third and fourth
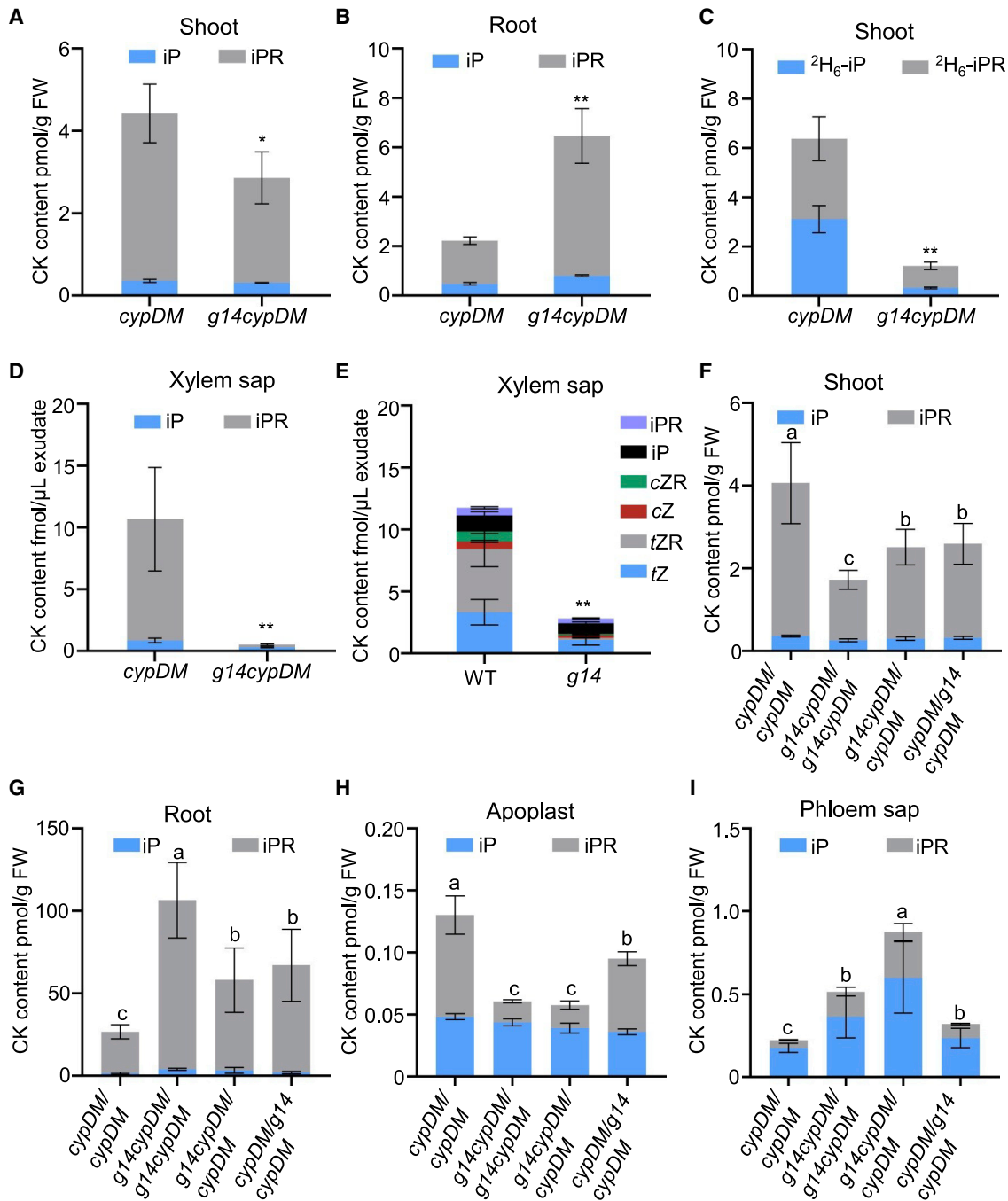
Figure 5. Shootward long-distance transport of iP-type CK species is mediated by AtABCG14.
(A and B) Quantification of iP-type CKs in the shoot **(A)** and root **(B)** of *cypDM* and *atabcg14 cypDM*. The seedlings were grown on half-strength Murashige and Skoog agar medium for 8 days before harvest of shoots and roots.
(C) Translocation of exogenous iP and iPR in *atabcg14 cypDM*. Roots of 8-DAG *cypDM* and *atabcg14 cypDM* seedlings were incubated with 50 nM $^2H_6$-iP for 1 h. The shoots were harvested for CK quantification.
(D and E) CK concentrations of xylem sap in *cypDM*, *atabcg14 cypDM* **(D)**, WT, and *atabcg14* **(E)**. Xylem sap was collected from 25-DAG plants.
(F–I) Quantification of CK content in the shoots **(F)**, roots **(G)**, apoplast **(H)**, and phloem sap **(I)** of *cypDM/cypDM*, *atabcg14 cypDM/atabcg14 cypDM*, *atabcg14 cypDM/cypDM*, and *cypDM/atabcg14 cypDM* plants at 25 DAG.
Data are means ± SD. $n = 3$ in **(A)–(E)** and **(I)**, $n = 4$ in **(F)–(H)**. Groups marked with different letters are significantly different ($P < 0.05$, ANOVA). *$P < 0.05$, **$P < 0.01$ (Student's *t*-test).

rosette leaves from 25-DAG plants of *cypDM* and *atabcg14 cypDM*. After 6 h, $^2H_6$-iP and $^2H_6$-iPR were quantified in the third and fourth leaves, younger leaves (fifth to tenth), and roots of

cypDM and *atabcg14 cypDM* plants (Figure 6A–6D). The levels of $^2H_6$-iP and $^2H_6$-iPR in *atabcg14 cypDM* younger leaves and roots were significantly reduced by 53% and 66% compared

with those in *cypDM* plants (Figure 6B and 6C), whereas they were similar in the third and fourth leaves (Figure 6D), suggesting that AtABCG14 was involved in phloem transport of iP-type CKs. We also detected $^2H_6$-iP and $^2H_6$-iPR contents in roots and younger leaves of WT and *atabcg14* after dripping $^2H_6$-iP onto the third and fourth leaves. $^2H_6$-iP and $^2H_6$-iPR contents of younger leaves (fifth to tenth) and roots of *atabcg14* were decreased by 28% and 58% compared with those of the WT (Supplemental Figure 10). The reduction in $^2H_6$-iP and $^2H_6$-iPR in the roots of *atabcg14 cypDM* and *atabcg14* indicated that AtABCG14 is involved in iP-type CK transport from shoot to root.

To more precisely elucidate how AtABCG14 is involved in shoot-to-root transport of iP-type CKs, we analyzed CKs in the phloem sap of *cypDM* and *atabcg14 cypDM*. The levels of iP and iPR in *atabcg14 cypDM* were significantly increased 1.9- and 1.8-fold, respectively, compared with those in *cypDM* (Figure 6E). The levels of iP and iPR in phloem sap were much higher in *atabcg14* than in the WT (Figure 6F). These data imply that disruption of AtABCG14 affected phloem unloading and reduced rootward translocation of iP-type CKs. Next, long-distance transport of iP-type CKs from shoot to root was detected in the grafted plants *cypDM/cypDM*, *atabcg14 cypDM/atabcg14 cypDM*, *atabcg14 cypDM/cypDM*, and *cypDM/atabcg14 cypDM* (Figure 6G). $^2H_6$-iP was dripped onto the third and fourth rosette leaves of the grafted plants. After 6 h, $^2H_6$-iP and $^2H_6$-iPR were measured in roots of the *atabcg14 cypDM/atabcg14 cypDM* and *cypDM/atabcg14 cypDM* plants, which lacked *AtABCG14* expression in the rootstock. The iP-type CK levels were significantly lower in *atabcg14 cypDM/atabcg14 cypDM* and *cypDM/atabcg14 cypDM* than in *cypDM/cypDM* and *atabcg14 cypDM/cypDM*, which did express *AtABCG14* in the rootstock (Figure 6G). Therefore, AtABCG14 is likely to play an important role in iP-type CK unloading in the root. $^2H_6$-iP and $^2H_6$-iPR levels appeared similar in roots of the grafted plants *cypDM/cypDM* and *atabcg14 cypDM/cypDM* (Figure 6G), suggesting that AtABCG14 is not necessary for phloem loading of iP-type CKs in the shoot.

Finally, we performed a split-root experiment using the $^2H_6$-iP tracer to determine whether iP-type CKs can move from the root to the shoot and then retrograde to the root (Figure 6H and 6I). Split roots of WT plants were incubated with or without $^2H_6$-labeled iP (Figure 6H). After 4 h, $^2H_6$-labeled iP and iPR were quantified in the shoot and the root that had not received $^2H_6$-labeled iP. The results showed that isotope-labeled CKs were transported to the shoot and then retrograded to the portion of the root system that had not received the $^2H_6$-iP tracer (Figure 6I). By contrast, the concentration of isotope-labeled CKs transported to the untreated roots was significantly reduced when the shoot was removed (Supplemental Figure 11). These results suggest that iP-type CKs can move from the root to the shoot and then retrograde to the root.

DISCUSSION

Long-distance transport and short-range cellular transport of CKs play essential roles in CK signaling and regulate multiple physiological processes (Duran-Medina et al., 2017; Kang et al., 2017; Anfang and Shani, 2021). Mechanisms for shootward

long-distance transport of *tZ*-type CKs in *Arabidopsis* or rice mediated by AtABCG14 or OsABCG18 have been addressed previously at the physiological level (Ko et al., 2014; Zhang et al., 2014; Zhao et al., 2019, 2021). Here we found that AtABCG14 can form a homodimer and display transporter activity toward multiple CKs. We revealed that iP-type CKs can move from the root to the shoot and then back to the root, confirming round-trip transport of iP-type CKs in *Arabidopsis*. In this process, AtABCG14 forms a homodimer and mediates root xylem loading and shoot phloem unloading in the shootward long-distance transport of iP-type CKs; it is also required for root phloem unloading in the rootward transport of iP-type CKs. We therefore propose a model for circular long-distance transport of iP-type CKs, which is systemically mediated by AtABCG14 in the root and shoot (Figure 7).

As a half-size ABC transporter involved in CK transport, AtABCG14 must form a homodimer or heterodimer to perform transport activities, but its partner and transport substrates remain to be characterized (Ko et al., 2014; Zhang et al., 2014). In this study, reciprocal coIP of FLAG-AtABCG14 and Myc-AtABCG14 fusion proteins expressed in Human HEK293T cells showed that AtABCG14 formed homodimers (Figure 1A). CoIP of GFP-AtABCG14 and Myc-AtABCG14 confirmed this conclusion in tobacco leaves and *atabcg14* mutants expressing *GFP-* and *Myc-AtABCG14* (Figure 1B and 1C). By contrast, an earlier report showed that the fusion proteins Myc-AtABCG14 and HA-AtABCG14 failed to form homodimers (Le Hir et al., 2013). This inconsistency may be caused by the fusion tags on AtABCG14 that could affect dimerization of AtABCG14 *in vivo*. AtABCG14 has been reported to form a heterodimer with AtABCG11 (Le Hir et al., 2013). A recent study showed that CKs overaccumulate in roots of the *atabcg11* mutant and that its root growth is insensitive to CK treatment, but whether AtABCG11 is directly involved in CK translocation remains to be determined (Yang et al., 2022).

On the other hand, transporter activities of AtABCG14 were measured in BY2 cells, *Arabidopsis* suspension cells, and cells of a non-plant system, yeast YPH499. These results clearly showed that AtABCG14 is directly involved in transport of multiple CK substrates, including *tZR*, iPR, *tZ*, and iP (Figures 2 and 3), suggesting that AtABCG14 prefers both the free and riboside-conjugated forms of *tZ*- and iP-type CKs as substrates. This is consistent with the fact that free and riboside-conjugated CKs are prominent forms in the long-distance transport of CKs (Sakakibara, 2020). By contrast, CK transporters such as PUP14 and AZG2, which are involved in short-range cellular translocation, prefer free forms of CKs (Zurcher et al., 2016; Tessi et al., 2020). Thus, the biochemical properties of AtABCG14 suggest that it plays essential roles in long-distance transport of multiple CKs.

AtABCG14 is expressed in nearly all cells in the root stele, including phloem and procambial cells (Ko et al., 2014; Zhang et al., 2014; Supplemental Figure 12), as well as xylem and phloem cells in the leaves (Zhao et al., 2021). AtABCG14 displayed transporter activity toward multiple CK species (Figures 2 and 3). These characteristics enable AtABCG14 to function as an efflux transporter at multiple steps in the long-distance transport of different CK species. The *cypDM* mutant fails
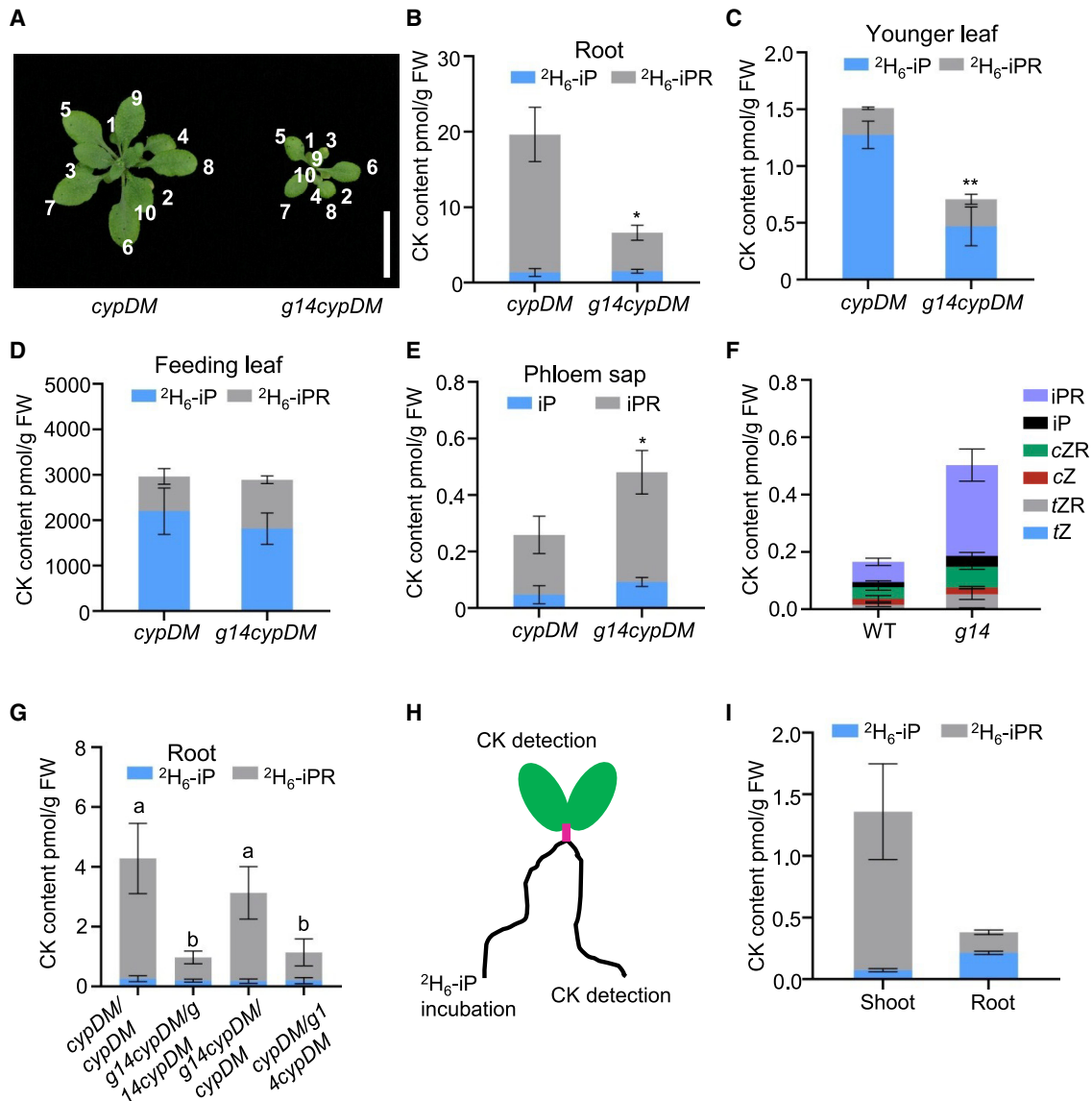
Figure 6. Rootward long-distance transport of iP-type CKs is mediated by AtABCG14.

(A) Morphological phenotypes of 25-DAG *cypDM* and *atabcg14 cypDM*. Scale bars, 1.5 cm. A solution of 5 ppm $^2H_6$-iP was dripped onto the third and fourth leaves of plants (7 μl/cm^2 leaf area) and incubated for 6 h. The roots **(B)**, younger (fifth to tenth) leaves **(C)**, and third and fourth leaves **(D)** were then harvested for CK quantification.

(E and F) Quantification of iP and iPR content in phloem sap of *cypDM*, *atabcg14 cypDM* **(E)**, WT, and *atabcg14* **(F)**. Phloem sap from 25-DAG plants was collected for CK quantification.

(G) A solution of 5 ppm $^2H_6$-iP was dripped onto the third and fourth leaves of 25-DAG plants and incubated for 6 h. The roots were harvested for CK quantification.

(H) WT plants were incubated under split-root conditions with or without $^2H_6$-labeled iP.

(I) Quantification of $^2H_6$-labeled iP and iPR contents in the shoot and untreated root (which did not receive $^2H_6$-labeled iP) after feeding with $^2H_6$-iP for 4 h in **(H)**.

Data are means ± SD. $n = 3$ in **(B)–(E)**, $n = 4$ in **(F), (G), and (I)**. *$P < 0.5$, **$P < 0.01$ (Student's *t*-test). Groups marked with different letters are significantly different ($P < 0.05$, ANOVA).

to produce *t*Z-type CKs (Kiba et al., 2013), making it ideal for studying iP-type CK transport without interference from *t*Z-type CKs. The triple mutant *atabcg14 cypDM* displayed shorter roots and less chlorophyll than *cypDM* and *atabacg14* plants (Figure 4A–4C). Hormone profiling and isotope tracing experiments showed that iP-type CKs transported from root to shoot were significantly suppressed in *atabcg14 cypDM* (Figure 5A–5E),

suggesting that AtABCG14 is essential for shootward long-distance transport of iP-type CKs. On the other hand, levels of leaf apoplastic iP-type CKs in *atabcg14 cypDM/atabcg14 cypDM* appeared to be similar to those in *atabcg14 cypDM/cypDM* but lower than those in *cypDM/cypDM* and *cypDM/atabcg14 cypDM* (Figure 5H). Levels of phloem sap iP-type CKs were up to 4-fold higher in *atabcg14 cypDM/cypDM* than in *cypDM/cypDM*
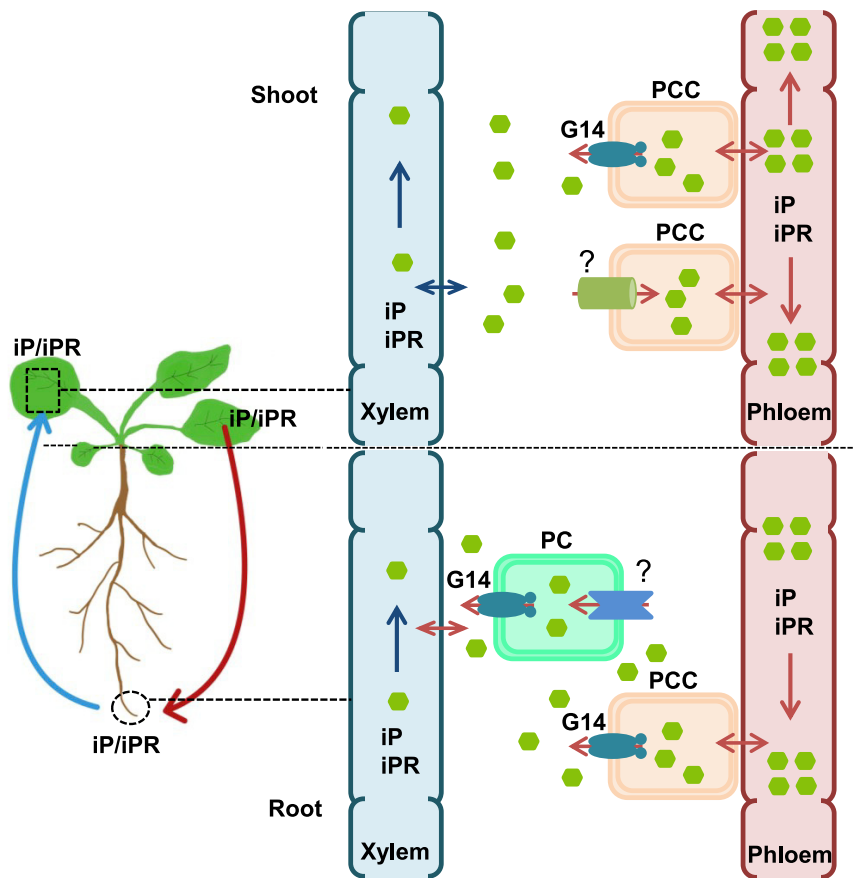
Figure 7. Diagram of AtABCG14-mediated circular long-distance transport of iP-type CKs.

In the root, iPR/iP produced in pericycle cells (PCs) or retrieved from the apoplast by an unknown transporter (?) are loaded into the root xylem by G14 (AtABCG14) on the PC PM. Then iPR/iP are transported via the xylem in the leaf transpiration stream. In the shoot, iPR/iP released from the xylem or synthesized in the shoot are loaded into the phloem companion cells (PCCs) in the stems or leaf veins by an unknown transporter (?). iPR/iP in the phloem are then transported upstream to the leaf minor veins and unloaded into the apoplast by G14 on the PCC PM for shoot distribution. iPR/iP in the phloem are transported downstream to the root. In the root, iPR/iP are unloaded from the phloem to the apoplast by G14 on the PCC PM. Finally, the released iPR/iP can be used for another round of circular long-distance transport.

verifying that AtABCG14 is involved in iP-type CK unloading in the root.

Consistent with the transporter activities of AtABCG14 toward multiple CK substrates, CK profiling in *atabcg14* and WT plants revealed that AtABCG14 was involved in long-distance transport of various CKs between the root and shoot. Levels of total CKs (*t*Z, *t*ZR, iP, iPR, *c*Z, and *c*ZR) were significantly lower in xylem sap but higher in phloem sap of the *atabcg14* mutant than in that of WT plants (Figures 5E and 6F), indicating that root-to-shoot and shoot-to-root transport of CKs were impaired by *AtABCG14* disruption. Compared with the WT, levels of iP-type CKs were consistently lower in xylem sap but higher in phloem sap of *atabcg14* plants (Figures 5E and 6F), consistent with the results obtained using *atabcg14 cypDM* and *cypDM* plants. Traditionally, root-derived tZ-type CKs are synthesized and transported from root to shoot, and, vice versa, shoot-derived iP-type CKs are synthesized in the shoot and transported from shoot to root (Hirose et al., 2007; Sakakibara, 2020). However, quantification of CKs in sap of the xylem and phloem showed that iP-type CKs also exist in xylem sap and that *t*Z-type CKs also exist in phloem sap (Figures 5E and 6F). CK quantification showed that levels of iP-type and *t*Z-type CKs were lower in xylem sap but higher in phloem sap of *atabcg14* than in that of the WT (Figures 5E and 6F). Thus, we speculate that root-to-shoot and shoot-to-root transport of *t*Z- and iP-type CKs are occurring and that AtABCG14 participates in both transport processes. A split-root experiment using isotope-labeled iP showed that iP-type CKs were transported from root to shoot and then retrograded from shoot to root (Figure 6H and 6I). This result is consistent with our previous observation that *t*Z-type CK can be retrograded to the root (Zhao et al., 2021), demonstrating that multiple CKs can be transported in the vascular system of *Arabidopsis*.

(Figure 5I), suggesting that AtABCG14 is required for shoot distribution of root-derived iP-type CKs. We have provided evidence of shootward long-distance transport of iP-type CKs, in which AtABCG14 is necessary for substrate loading and distribution. Previous studies have shown that AtABCG14 is essential for shootward long-distance translocation and shoot distribution of root-synthesized *t*Z-type CKs (Ko et al., 2014; Zhang et al., 2014; Zhao et al., 2021). These results reveal that AtABCG14 is involved in shootward long-distance transport of multiple CKs *in vivo*.

Previous studies have suggested that iP-type CKs transported from shoot to root via the phloem regulate root development and nodulation in *Arabidopsis* or *Lotus japonicus* (Bishopp et al., 2011; Sasaki et al., 2014; Sakakibara, 2020); however, the transporters involved in long-distance transport of iP-type CKs have not yet been found. In this work, we show that AtABCG14 is responsible for phloem unloading of iP-type CKs in their shoot-to-root transport (Figure 6 and Supplemental Figure 10). ²H₆-iP tracer experiments showed that the levels of ²H₆-iP and ²H₆-iPR transported from roots to younger rosette leaves were also significantly decreased in the absence of AtABCG14 (Figure 6B and 6C). CK profiling in the phloem sap showed that more iP-type CKs accumulated in the phloem of *atabcg14 cypDM* than of *cypDM* (Figure 6E). These results imply that AtABCG14 is required for rootward transport of iP-type CKs. Grafting experiments showed that rootward iP-type CKs were reduced by 73% when *AtABCG14* was disrupted in the *atabcg14 cypDM* rootstock (Figure 6G),

We revealed that iP-type CKs exhibit circular transport in the vascular system. AtABCG14 has various roles, including root

xylem loading, shoot phloem unloading, and root phloem unloading of cargoes in circular long-distance transport of iP-type CKs (Figure 7). The biological significance of this process may be that recirculation of CKs in the vascular system would facilitate rapid delivery of hormones in response to growth and stress signals. After exposure to environmental stimuli, it is much faster for CKs to travel to the target cells from the nearby vascular system than from their original synthesis sites. This circular transport could be a universal mechanism for other hormones or signals in plants, enabling them to respond quickly to internal and external stimuli. These findings provide new insights into CK transport and, possibly, into the transport of other plant hormones. The transporters responsible for phloem loading of iP-type CKs in shoot-to-root long-distance transport remain to be characterized.

METHODS

Plant materials and growth conditions

The *A. thaliana* Col-0 ecotype was used as the WT. *cypDM* was obtained by crossing *cyp735a1* and *cyp735a2* (SALK_093028C and SALK_077856C from *Arabidopsis* Biological Resource Center) . The *atabcg14* mutant, *35S::GFP-AtABCG14* transgenic plants, and *AtABCG14pro::GUS* transgenic plants have been described previously (Zhang et al., 2014). The transgenic plants co-expressing *SUC2pro::mCherry* and *AtABCG14pro::eGFP* have been described previously (Zhao et al., 2021). The *4CL1pro::mCherry* transgenic plants were generated using the floral dip method (Clough and Bent, 1998). Plants co-expressing *4CL1pro::mCherry* and *AtABCG14pro::eGFP* were obtained by crossing *4CL1pro::mCherry* and *AtABCG14pro::eGFP* transgenic plants. *atabcg14 cypDM* triple mutant was generated by crossing *cypDM* and *atabcg14* and was characterized using the primers described in Supplemental Table 1 (AtCYP735A1-P1, P2 and LB1.3 for the *cyp735a1* mutant; AtCYP735A2-P1, P2 and LB1.3 for the *cyp735a2* mutant; AtABCG14-P7, P8 and AtABCG14-P11, pSKTAIL for the *atabcg14* mutant). Seeds were sown on Petri dishes containing half-strength Murashige and Skoog medium (M519; PhytoTechnology Laboratories, Shawnee Mission, KS, USA) and 0.5% (w/v) gellan gum (G434; PhytoTechnology Laboratories, Shawnee Mission, KS, USA). The seeds were incubated at 4°C for 3 days and then transferred to a growth chamber. Seedlings with two true leaves were transplanted into soil (Professional Growing Mix; Sun Gro Horticulture Canada, Seba Beach, AB T0E 2B0, Canada) and grown under a 16-h light/8-h dark cycle and ~60% relative humidity unless otherwise indicated. The light intensity was ~110 μmol m^{-2} s^{-1}. The WT, mutant, and/or transgenic plants were grown in parallel in the same trays to minimize variations in the growth conditions.

CoIP and gel blot analysis

For coIP, human HEK293T cells (from the China Center for Type Culture Collection) co-transfected with the *FLAG-AtABCG14* and *Myc-AtABCG14* vectors were lysed with 500 μl NP-40 buffer (1× PBS, 0.5% NP-40, 0.5% proteinase inhibitor cocktail) for 10 min. The lysates were centrifuged at 4°C and 12 000 g for 5 min. The supernatants were incubated with FLAG (F3165, Sigma) or Myc (M4439, Sigma) antibodies (1:100 dilution) at room temperature for 2 h and further incubated with protein G beads (17-0618-01, GE) for 1 h. The beads were washed three times with NP-40 buffer. Samples were boiled in 1× SDS sample buffer for 5 min and detected by western blotting. Tobacco (*N. benthamiana*) leaves and *Arabidopsis* transformed with *GFP-AtABCG14* and *Myc-AtABCG14* were homogenized in protein buffer (100 mM Tris-HCl [pH 8.0], 150 mM NaCl, 1× proteinase inhibitor, 0.05% Triton X-100). The lysates were centrifuged at 4°C and 12 000 g for 10 min. The supernatants were incubated with GFP beads (GFP-Trap_A, gta-20, Chromotek) for 1 h. The beads were then surface washed three times with protein buffer. Samples were boiled in 1× SDS sample buffer for 5 min and detected by western blotting.

For immunoblotting, the samples were probed with a 1:1000 dilution of GFP antibodies (A-6455, Invitrogen), 1:2000 dilution of Myc antibodies (M4439, Sigma) or FLAG (F3165, Sigma). The secondary antibodies were goat anti-rabbit (AS09 633, Agrisera) for GFP, and goat anti-mouse (BS12478, Bbioworlde) for Myc and FLAG . The signals were detected using the Tanon Imaging System (Tanon 6600).

Plasmid construction

For the transport activity assay in yeast, the GFP-AtABCG14 coding sequence in pSAT6-GFP-AtABCG14 (Zhang et al., 2014) was amplified with the AtABCG14-P3 and AtABCG14-P4 primers. It was cloned into the pDR195 vector (Li et al., 2020) using the sequence- and ligation-independent cloning method (Jeong et al., 2012). For the AtABCG14 coIP assay in human HEK293T cells, the AtABCG14 fragment was amplified by AtABCG14-P9 and AtABCG14-P10 primers from pSAT6-GFP-AtABCG14 (Zhang et al., 2014), digested with *Xba*I, and then ligated into the pCS2 vector (Jin et al., 2010) digested by *Stu*I and *Xba*I to obtain the Myc-AtABCG14-pCS2 and FLAG-AtABCG14-pCS2 plasmids. For the AtABCG14 coIP assays in transgenic tobacco and *Arabidopsis*, the GFP-AtABCG14-RCS2 vector and GFP-AtABCG14-RCS2 transgenic plants described in previous research (Zhang et al., 2014) were used. Fragments of *Myc-AtABCG14* and *FLAG-AtABCG14* were amplified from the Myc-AtABCG14-pCS2 vector with AtABCG14-P1 and AtABCG14-P2 primers, ligated into the PCR8 vector (Invitrogen) using the sequence- and ligation-independent cloning method, and finally cloned into the binary vector pMDC32 (Curtis and Grossniklaus, 2003) by the LR reaction using Gateway LR Clonase II enzyme mix (11791-020, Invitrogen). For *4CL1pro::mCherry* transgenic plants, 4CL1pro-pDONR207 was ligated to pMDC163-mCherry using the LR reaction to obtain pMDC163-4CL1pro-mCherry. All primers are listed in Supplemental Table 1.

Gene transcription analysis

Total RNA was extracted with a MiniBEST Universal RNA Extraction Kit (9767, TaKaRa Bio, Kusatsu, Shiga, Japan). cDNA was synthesized with HiScript qRT Supermix for qPCR (+gDNA Wiper) (R123-01, Vazyme Biotech, Nanjing, China). qRT–PCR was performed using SYBR Green (TaKaRa Bio, Kusatsu, Shiga, Japan) on a qTOWER 2.2 real-time PCR thermal cycler (Analytik Jena, Germany). *ACTIN2* was used as the internal control for qRT–PCR data analysis. The qRT–PCR primers are listed in Supplemental Table 1. The transcript levels of the target genes were normalized to that of *ACTIN2*.

Hormone quantification

CKs and ABA were extracted, quantified, and analyzed using a previously described method (Cao et al., 2015; Zhao et al., 2021). In brief, the hormones were extracted using 80% methanol with internal standards (i.e., 45 pg [^{2}H$_6$]iP and [^{2}H$_6$]iPR or 250 pg [^{2}H$_6$]ABA); after drying with nitrogen gas, the pellet was dissolved in 300 μl 30% (v/v) methanol. After centrifugation, the supernatant was passed through a 0.22-μm membrane filter and used for CK quantification. The CKs and ABA were separated with the LC (ExionLC^{TM},AB SCIEX) and analyzed with the triple quadruple MS QTRAP 5500 system (AB SCIEX). The data were processed using MultiQuant software (version 3.0.2, AB SCIEX).

Transporter activity assays using *AtABCG14*-expressing BY-2 cells and *Arabidopsis* cells

Transformation of BY-2 cells with the *35S::GFP* and *35S::GFP-AtABCG14* vectors was performed according to methods described previously (Staub, 2014). The suspension cells were prepared by transferring calli transformed with the *35S::GFP* and *35S::GFP-AtABCG14* vectors to liquid medium. The liquid medium contains 4.3 g/l Murashige and Skoog basal salts (M524; PhytoTechnology Laboratories, Shawnee Mission, KS, USA), 30 g/l sucrose, 0.18 g/l KH$_2$PO$_4$, 0.001 g/l thiamine, 0.1 g/l myo-inositol, 0.001 mM 2,4-dichlorophenoxyacidic acid (A600166-0100, Sangon Biotech, China), and 20 mg/l hygromycin B (CH6361, Coolaber, China),

adjusting the pH to 5.7. After 7 days of growth, 1 ml of BY-2 cells transformed with *35S::GFP* and *35S::GFP-AtABCG14* were transferred to 20 ml of new medium for subculture. The BY-2 cells were subcultured three times and then used for the transport activity assay. One milliliter of BY-2 cells transformed with *35S::GFP* and *35S::GFP-AtABCG14* were transferred to 20 ml of new medium and grown for 5 days. For CK quantification, 500 μl of liquid medium was collected following the methods described above. About 0.1 g of BY-2 cells transformed with *35S::GFP* and *35S::GFP-AtABCG14* were collected for CK extraction and quantification following the methods described above.

WT and *35S::GFP-AtABCG14 Arabidopsis* calli were induced from the root segments of *Arabidopsis* seedlings using methods described previously (Li et al., 2020). The culture of suspension cells was initiated by transferring the calli to B5 liquid medium (Gamborg's B-5 medium, HB8487-2, Qingdao Hope Bio-Technology, China) supplemented with 30 g/l sucrose and 1 mg/l 2,4-dichlorophenoxyacetic acid, adjusting the pH to 5.7. After 7 days of growth, 2 ml of *Arabidopsis* cells were transferred to 20 ml of new medium for subculture. The *Arabidopsis* cells were subcultured three times and then used for the transport activity assay. One milliliter of suspension cells were transferred to 20 ml of new medium and grown for 5 days. Two milliliters of WT and *35S::GFP-AtABCG14 Arabidopsis* cells were transferred to 10 ml of new medium and incubated for 0.5, 1, 2, 4, and 8 h. For CK quantification, 500 μl of liquid medium was collected following the methods described above. Approximately 0.1 g of *Arabidopsis* cells were collected for CK extraction and quantification following the methods described above.

Transporter activity assay in yeast cells

CK transport experiments were performed as follows. Yeast YPH499 cells (optical density 600 [OD_{600}] = 0.6) grown in yeast medium (6.7 g/l yeast nitrogen base [A610507, Sangon Biotech, China], 20 g/l glucose, and 0.77 g/l –uracil dropout supplement [630416, TaKaRa Bio, USA]) were harvested, washed twice with uptake buffer (100 mM potassium phosphate buffer [pH 5.8]), re-suspended in the same buffer to a final OD_{600} of 50, and kept on ice for use in uptake assays. The 0.2-ml cell suspensions for one sample were pre-incubated at 28°C for 2 min and then incubated in 0.2 ml uptake buffer with ^{2}H-labeled *tZ*, *tZR*, iP, iPR, DHZ, and ^{15}N-labeled *cZ* (50 nM, OlChemIm, Olomouc, Czech Republic) at 28°C for 20 min. After centrifugation (15 s, 10 000 g), the yeast cells were quickly surface washed with 1.5 ml uptake buffer and then centrifuged (15 s, 10 000 g) to collect the yeast cells for CK extraction and quantification. For CK extraction, 500 μl 80% methanol and 0.2 g glass beads (A500478-0050, Sangon Biotech, China) were added to 2.0-ml tubes containing yeast cells, and the tubes were placed under severe vortex movement for 90 s for cell breakage. After centrifugation (10 min, 15 000 g, 4°C), the supernatant was passed through a 0.22-μm membrane filter, and 300 μl was used for CK quantification following the methods described above. For the efflux transport assay, the yeast cells were incubated in 0.2 ml uptake buffer with ^{2}H-labeled *tZ* at 28°C for 20 min. After centrifugation (15 s, 10 000 g), the yeast cells were quickly surface washed with 1.5 ml uptake buffer and then centrifuged (15 s, 10 000 g) to collect the yeast cells for the efflux transport assay. The yeast cells were resuspended in 1 ml incubation buffer (100 mM potassium phosphate buffer [pH 5.8]). After incubation for 0, 2, 4, 6, and 8 min at 28°C, 200 μl solution was collected for CK quantification by LC-MS/MS.

Micro-grafting and chlorophyll assay

The *Arabidopsis* micro-graft method from a previous protocol was used (Zhao et al., 2021). Chlorophyll was extracted from shoots of 10-DAG seedlings of Col-0, *atabcg14*, *cypDM*, and *atabcg14 cypDM* and quantified as described previously (Zhang et al., 2017).

Isotope tracer experiments

Isotope (^{2}H$_6$-iP) tracer experiments were performed as described previously (Zhang et al., 2014). 8-DAG seedlings were used to trace the

shootward transport of the ^{2}H$_6$-iP isotope. Roots were immersed in 5 mM MES-KOH (morpholineethanesulfonic acid-potassium hydroxide) (pH 5.6) buffer containing ^{2}H$_6$-iP (final concentration, 50 nM; OlChemIm, Olomouc, Czech Republic) under normal growth conditions for 1 h. The roots were washed with distilled water twice to remove the solution on the surface. CKs were then extracted from the roots and shoots and quantified according to the method described above, using [^{15}N$_4$] *cZ* (OlChemIm, Olomouc, Czech Republic) as an internal standard.

To trace ^{2}H$_6$-iP transport from shoot to root or from adult leaves to younger leaves, experiments were performed using 25-DAG plants as follows. Five millimolar MES-KOH (pH 5.6) buffer containing ^{2}H$_6$-iP (final concentration, 20 μM) and 0.1% (v/v) Triton X-100 was dripped onto the third and fourth leaves of the WT, *atabcg14*, *cypDM*, and *atabcg14 cypDM* (approximately 7.0 μl/cm^2) and incubated for 6 h. The third and fourth leaves, fifth and sixth leaves, and roots from one (Col-0), two (*atabcg14*, *cypDM*), or four (*atabcg14 cypDM*) plants were harvested as one biological replicate for CK extraction and quantification according to the method described above. [^{15}N$_4$]*cZ* was used as an internal control.

The split-root experiment followed a previous protocol (Poitout et al., 2018). In brief, plants were grown on half-strength Murashige and Skoog medium. On day 10, the primary root was cut off below the second lateral root to obtain two new primary roots. On day 20, plants with the shoot or with the shoot removed were transferred to half-strength Murashige and Skoog medium with or without 50 nM ^{2}H$_6$-iP. After 4 h, the shoots and untreated roots were collected for CK extraction.

SUC2$_{pro}$-mCherry, 4CL1$_{pro}$-mCherry, and AtABCG14$_{pro}$-GFP co-expression

10-DAG seedlings harboring pMDC163-SUC2$_{pro}$-mCherry and pMDC 107-AtABCG14$_{pro}$-GFP or pMDC163-4CL1$_{pro}$-mCherry and pMDC107-AtABCG14$_{pro}$-GFP were observed under an LSM 880 confocal microscope system (Carl Zeiss, Jena, Germany) using the following excitation or emission settings: 488 nm/505–550 nm for GFP and 561 nm/600–660 nm for mCherry. Images were processed using LSM image processing software (Carl Zeiss).

Phloem sap, apoplast, and xylem sap extraction

Phloem sap and apoplasts were extracted and quantified according to a previous protocol (Tetyuk et al., 2013; Zhao et al., 2021). Xylem sap was collected as described previously (Ko et al., 2014) with minor modifications. The shoots of 25-DAG plants were excised using a blade at the hypocotyl. The xylem sap was collected using a filter for 2 h after decapitation of the shoot. The total CKs in the sap were extracted with 300 μl 30% methanol and measured following the methods described above.

Statistical analyses

Two-tailed Student's *t*-test and one-way analysis of variance (least significant difference test) were used to analyze differences between plants and/or treatments in SPSS v.13.0 (IBM, Armonk, NY, USA). Different letters above the bars indicate significant differences ($P < 0.05$) according to the least significant difference test.

ACCESSION NUMBERS

Sequence data from this article can be found in the Arabidopsis Genome Initiative database under the following accession numbers: *AtABCG14* (AT1G31770), *CYP735A1* (AT5G38450), *CYP735A2* (AT1G67110), *At-SUC2* (AT1G22710), *At4CL1* (AT1G51680), and *ACTIN2* (AT3G18780).

SUPPLEMENTAL INFORMATION

Supplemental information is available at *Plant Communications Online*.

AUTHOR CONTRIBUTIONS

K.Z., J.Z., C.-J.L., and Z.J. conceived and designed the experiments. K.Z. supervised the study. J.Z., J.L., and J.Q. conducted the coIP assay. J.Z., M.J., T.L., and J.Q. conducted the transport activity assay. X.D. conducted the gene expression analysis. J.Z., X.D., J.Q., T.L., X.Z., and Q.Y. conducted the phenotype analysis and cytokinin profiling. J.Z. and X.D. conducted the grafting experiment. J.Z., X.D., and T.L. conducted tracer experiments and the apoplast, xylem sap, and phloem sap assays. K.Z., J.Z., W.L., C.-J.L., and Z.J. analyzed the data and wrote the paper. All authors discussed the results and collectively edited the manuscript.

REFERENCES

Anfang, M., and Shani, E. (2021). Transport mechanisms of plant hormones. Curr. Opin. Plant Biol. **63**, 102055. https://doi.org/10.1016/j.pbi.2021.102055.

Ashikari, M., Sakakibara, H., Lin, S., Yamamoto, T., Takashi, T., Nishimura, A., Angeles, E.R., Qian, Q., Kitano, H., and Matsuoka, M. (2005). Cytokinin oxidase regulates rice grain production. Science **309**:741–745.

Banasiak, J., and Jasiński, M. (2021). ATP-binding cassette transporters in nonmodel plants. New Phytol. **233**:1597–1612.

Bartrina, I., Otto, E., Strnad, M., Werner, T., and Schmülling, T. (2011). Cytokinin regulates the activity of reproductive meristems, flower organ size, ovule formation, and thus seed yield in Arabidopsis thaliana. Plant Cell **23**:69–80. https://doi.org/10.1105/tpc.110.079079.

Bishopp, A., Lehesranta, S., Vatén, A., Help, H., El-Showk, S., Scheres, B., Helariutta, K., Mähönen, A.P., Sakakibara, H., and Helariutta, Y. (2011). Phloem-transported cytokinin regulates polar auxin transport and maintains vascular pattern in the root meristem. Curr. Biol. **21**:927–932.

Cao, Z., Ma, Y., Mou, R., Yu, S., and Chen, M. (2015). Analysis of 17 cytokinins in rice by solid phase extraction purification and liquid chromatography-tandem mass spectrometry. Chin. J. Chromatogr. **33**:715–721.

Clough, S.J., and Bent, A.F. (1998). Floral dip: a simplified method for Agrobacterium-mediated transformation of Arabidopsis thaliana. Plant J. **16**:735–743. https://doi.org/10.1046/j.1365-313x.1998.00343.x.

Cortleven, A., Leuendorf, J.E., Frank, M., Pezzetta, D., Bolt, S., and Schmülling, T. (2019). Cytokinin action in response to abiotic and biotic stresses in plants. Plant Cell Environ. **42**:998–1018. https://doi.org/10.1111/pce.13494.

Curtis, M.D., and Grossniklaus, U. (2003). A Gateway cloning vector set for high-throughput functional analysis of genes in planta. Plant Physiol. **133**:462–469. https://doi.org/10.1104/pp.103.027979.

Durán-Medina, Y., Díaz-Ramírez, D., and Marsch-Martínez, N. (2017). Cytokinins on the move. Front. Plant Sci. **8**:146. https://doi.org/10.3389/fpls.2017.00146.

Hirose, N., Takei, K., Kuroha, T., Kamada-Nobusada, T., Hayashi, H., and Sakakibara, H. (2007). Regulation of cytokinin biosynthesis, compartmentalization and translocation. J. Exp. Bot. **59**:75–83. https://doi.org/10.1093/jxb/erm157.

Hwang, I., and Sheen, J. (2001). Two-component circuitry in Arabidopsis cytokinin signal transduction. Nature **413**:383–389. https://doi.org/10.1038/35096500.

Hwang, I., Sheen, J., and Müller, B. (2012). Cytokinin signaling networks. Annu. Rev. Plant Biol. **63**:353–380. https://doi.org/10.1146/annurev-arplant-042811-105503.

Jasiński, M., Stukkens, Y., Degand, H., Purnelle, B., Marchand-Brynaert, J., and Boutry, M. (2001). A plant plasma membrane ATP binding cassette-type transporter is involved in antifungal terpenoid secretion. Plant Cell **13**:1095–1107. https://doi.org/10.1105/tpc.13.5.1095.

Jeong, J.-Y., Yim, H.-S., Ryu, J.-Y., Lee, H.S., Lee, J.-H., Seen, D.-S., and Kang, S.G. (2012). One-step sequence- and ligation-independent cloning as a rapid and versatile cloning method for functional genomics studies. Appl. Environ. Microbiol. **78**:5440–5443. https://doi.org/10.1128/aem.00844-12.

Jin, Z., Wallace, L., Harper, S.Q., and Yang, J. (2010). PP2A:B56ε, a substrate of caspase-3, regulates p53-dependent and p53-independent apoptosis during development. J. Biol. Chem. **285**:34493–34502. https://doi.org/10.1074/jbc.M110.169581.

Juan-Carlos, P.-D.M., Perla-Lidia, P.-P., Stephanie-Talia, M.-M., Mónica-Griselda, A.M., and Luz-María, T.E. (2021). ABC transporter superfamily. An updated overview, relevance in cancer multidrug resistance and perspectives with personalized medicine. Mol. Biol. Rep. **48**:1883–1901.

Kang, J., Lee, Y., Sakakibara, H., and Martinoia, E. (2017). Cytokinin transporters: GO and STOP in signaling. Trends Plant Sci. **22**:455–461. https://doi.org/10.1016/j.tplants.2017.03.003.

Kiba, T., Takei, K., Kojima, M., and Sakakibara, H. (2013). Side-chain modification of cytokinins controls shoot growth in Arabidopsis. Dev. Cell **27**:452–461. https://doi.org/10.1016/j.devcel.2013.10.004.

Kieber, J.J., and Schaller, G.E. (2018). Cytokinin signaling in plant development. Development **145**:dev149344. https://doi.org/10.1242/dev.149344.

Kim, A., Chen, J., Khare, D., Jin, J.-Y., Yamaoka, Y., Maeshima, M., Zhao, Y., Martinoia, E., Hwang, J.-U., and Lee, Y. (2020). Non-intrinsic ATP-binding cassette proteins ABCI19, ABCI20 and ABCI21 modulate cytokinin response at the endoplasmic reticulum in Arabidopsis thaliana. Plant Cell Rep. **39**:473–487. https://doi.org/10.1007/s00299-019-02503-0.

Ko, D., Kang, J., Kiba, T., Park, J., Kojima, M., Do, J., Kim, K.Y., Kwon, M., Endler, A., Song, W.Y., et al. (2014). Arabidopsis ABCG14 is essential for the root-to-shoot translocation of cytokinin. Proc. Natl. Acad. Sci. USA **111**:7150–7155. https://doi.org/10.1073/pnas.1321519111.

Kurakawa, T., Ueda, N., Maekawa, M., Kobayashi, K., Kojima, M., Nagato, Y., Sakakibara, H., and Kyozuka, J. (2007). Direct control of shoot meristem activity by a cytokinin-activating enzyme. Nature **445**:652–655. https://doi.org/10.1038/nature05504.

Kuroha, T., Tokunaga, H., Kojima, M., Ueda, N., Ishida, T., Nagawa, S., Fukuda, H., Sugimoto, K., and Sakakibara, H. (2009). Functional analyses of LONELY GUY cytokinin-activating enzymes reveal the

importance of the direct activation pathway in Arabidopsis. Plant Cell **21**:3152–3169. https://doi.org/10.1105/tpc.109.068676.

Lacombe, B., and Achard, P. (2016). Long-distance transport of phytohormones through the plant vascular system. Curr. Opin. Plant Biol. **34**:1–8. https://doi.org/10.1016/j.pbi.2016.06.007.

Le Hir, R., Sorin, C., Chakraborti, D., Moritz, T., Schaller, H., Tellier, F., Robert, S., Morin, H., Bako, L., and Bellini, C. (2013). ABCG9, ABCG11 and ABCG14 ABC transporters are required for vascular development in Arabidopsis. Plant J. **76**:811–824. https://doi.org/10.1111/tpj.12334.

Li, M., Wang, F., Li, S., Yu, G., Wang, L., Li, Q., Zhu, X., Li, Z., Yuan, L., and Liu, P. (2020). Importers drive leaf-to-leaf jasmonic acid transmission in wound-induced systemic immunity. Mol. Plant **13**:1485–1498. https://doi.org/10.1016/j.molp.2020.08.017.

Li, Q., Zheng, J., Li, S., Huang, G., Skilling, S.J., Wang, L., Li, L., Li, M., Yuan, L., and Liu, P. (2017). Transporter-mediated nuclear entry of jasmonoyl-isoleucine is essential for jasmonate signaling. Mol. Plant **10**:695–708. https://doi.org/10.1016/j.molp.2017.01.010.

Matsumoto-Kitano, M., Kusumoto, T., Tarkowski, P., Kinoshita-Tsujimura, K., Václavíková, K., Miyawaki, K., and Kakimoto, T. (2008). Cytokinins are central regulators of cambial activity. Proc. Natl. Acad. Sci. USA **105**:20027–20031. https://doi.org/10.1073/pnas.0805619105.

McFarlane, H.E., Shin, J.J.H., Bird, D.A., and Samuels, A.L. (2010). Arabidopsis ABCG transporters, which are required for export of diverse cuticular lipids, dimerize in different combinations. Plant Cell **22**:3066–3075.

Novák, O., Napier, R., and Ljung, K. (2017). Zooming in on plant hormone analysis: tissue- and cell-specific approaches. Annu. Rev. Plant Biol. **68**:323–348. https://doi.org/10.1146/annurev-arplant-042916-040812.

Poitout, A., Crabos, A., Petřík, I., Novák, O., Krouk, G., Lacombe, B., and Ruffel, S. (2018). Responses to systemic nitrogen signaling in Arabidopsis roots involve trans-zeatin in shoots. Plant Cell **30**:1243–1257.

Qi, Z., and Xiong, L. (2013). Characterization of a purine permease family GeneOsPUP7Involved in growth and development control in rice. J. Integr. Plant Biol. **55**:1119–1135. https://doi.org/10.1111/jipb.12101.

Rees, D.C., Johnson, E., and Lewinson, O. (2009). ABC transporters: the power to change. Nat. Rev. Mol. Cell Biol. **10**:218–227. https://doi.org/10.1038/nrm2646.

Sakakibara, H. (2005). Cytokinin biosynthesis and regulation. Vitam. Horm. **72**:271–287. https://doi.org/10.1016/s0083-6729(05)72008-2.

Sakakibara, H. (2020). Cytokinin biosynthesis and transport for systemic nitrogen signaling. Plant J. **105**:421–430. https://doi.org/10.1111/tpj.15011.

Sakamoto, T., Sakakibara, H., Kojima, M., Yamamoto, Y., Nagasaki, H., Inukai, Y., Sato, Y., and Matsuoka, M. (2006). Ectopic expression of KNOTTED1-like homeobox protein induces expression of cytokinin biosynthesis genes in rice. Plant Physiol. **142**:54–62. https://doi.org/10.1104/pp.106.085811.

Santner, A., Calderon-Villalobos, L.I.A., and Estelle, M. (2009). Plant hormones are versatile chemical regulators of plant growth. Nat. Chem. Biol. **5**:301–307. https://doi.org/10.1038/nchembio.165.

Sasaki, T., Suzaki, T., Soyano, T., Kojima, M., Sakakibara, H., and Kawaguchi, M. (2014). Shoot-derived cytokinins systemically regulate root nodulation. Nat. Commun. **5**:4983.

Šimura, J., Antoniadi, I., Široká, J., Tarkowská, D., Strnad, M., Ljung, K., and Novák, O. (2018). Plant hormonomics: multiple phytohormone profiling by targeted metabolomics. Plant Physiol. **177**:476–489. https://doi.org/10.1104/pp.18.00293.

Staub, J.M. (2014). Plastid transformation of tobacco suspension cell cultures. Methods Mol. Biol. **1132**:177–185. https://doi.org/10.1007/978-1-62703-995-6_10.

Tessi, T.M., Brumm, S., Winklbauer, E., Schumacher, B., Pettinari, G., Lescano, I., González, C.A., Wanke, D., Maurino, V.G., Harter, K., and Desimone, M. (2020). Arabidopsis AZG2 transports cytokinins in vivo and regulates lateral root emergence. New Phytol. **229**:979–993. https://doi.org/10.1111/nph.16943.

Tetyuk, O., Benning, U.F., and Hoffmann-Benning, S. (2013). Collection and analysis of Arabidopsis phloem exudates using the EDTA-facilitated Method. J. Vis. Exp. **80**, e51111. https://doi.org/10.3791/51111.

Xiao, Y., Liu, D., Zhang, G., Gao, S., Liu, L., Xu, F., Che, R., Wang, Y., Tong, H., and Chu, C. (2019). Big Grain3, encoding a purine permease, regulates grain size via modulating cytokinin transport in rice. J. Integr. Plant Biol. **61**:581–597. https://doi.org/10.1111/jipb.12727.

Xiao, Y., Zhang, J., Yu, G., Lu, X., Mei, W., Deng, H., Zhang, G., Chen, G., Chu, C., Tong, H., et al. (2020). Endoplasmic reticulum-localized PURINE PERMEASE1 regulates plant height and grain weight by modulating cytokinin distribution in rice. Front. Plant Sci. **11**:618560. https://doi.org/10.3389/fpls.2020.618560.

Yang, Q., Zhang, J., Kojima, M., Takebayashi, Y., Uragami, T., Kiba, T., Sakakibara, H., and Lee, Y. (2022). ABCG11 modulates cytokinin responses in Arabidopsis thaliana. Front. Plant Sci. **13**:976267.

Zhang, K., Novak, O., Wei, Z., Gou, M., Zhang, X., Yu, Y., Yang, H., Cai, Y., Strnad, M., and Liu, C.-J. (2014). Arabidopsis ABCG14 protein controls the acropetal translocation of root-synthesized cytokinins. Nat. Commun. **5**:3274. https://doi.org/10.1038/ncomms4274.

Zhang, Y., Zhao, L., Zhao, J., Li, Y., Wang, J., Guo, R., Gan, S., Liu, C.-J., and Zhang, K. (2017). S5H/DMR6 encodes a salicylic acid 5-hydroxylase that fine-tunes salicylic acid homeostasis. Plant Physiol. **175**:1082–1093. https://doi.org/10.1104/pp.17.00695.

Zhao, J., Yu, N., Ju, M., Fan, B., Zhang, Y., Zhu, E., Zhang, M., and Zhang, K. (2019). ABC transporter OsABCG18 controls the shootward transport of cytokinins and grain yield in rice. J. Exp. Bot. **70**:6277–6291. https://doi.org/10.1093/jxb/erz382.

Zhao, J., Ding, B., Zhu, E., Deng, X., Zhang, M., Zhang, P., Wang, L., Dai, Y., Xiao, S., Zhang, C., et al. (2021). Phloem unloading via the apoplastic pathway is essential for shoot distribution of root-synthesized cytokinins. Plant Physiol. **186**:2111–2123. https://doi.org/10.1093/plphys/kiab188.

Zürcher, E., Liu, J., di Donato, M., Geisler, M., and Müller, B. (2016). Plant development regulated by cytokinin sinks. Science **353**:1027–1030. https://doi.org/10.1126/science.aaf7254.